

Time resolved tracking of a sound scatterer in a complex flow: non-stationary signal analysis and applications

Nicolas Mordant and Jean-François Pinton*
École Normale Supérieure de Lyon & CNRS UMR 5672,
Laboratoire de Physique
46, allée d'Italie, F-69364 Lyon, France

Olivier Michel
Université de Nice
Laboratoire d'astrophysique & CNRS UMR 5525,
Parc Valrose, F-06108 Nice, France
 (Dated: October 26, 2018)

It is known that ultrasound techniques yield non-intrusive measurements of hydrodynamic flows. For example, the study of the echoes produced by a large number of particles insonified by pulsed wavetrains has led to a now standard velocimetry technique. In this paper, we propose to extend the method to the continuous tracking of one single particle embedded in a complex flow. This gives a Lagrangian measurement of the fluid motion, which is of importance in mixing and turbulence studies. The method relies on the ability to resolve in time the Doppler shift of the sound scattered by the continuously insonified particle.

For this signal processing problem two classes of approaches are used: time-frequency analysis and parametric high resolution methods. In the first class we consider the spectrogram and reassigned spectrogram, and we apply it to detect the motion of a small bead settling in a fluid at rest. In more non-stationary turbulent flows where methods in the second class are more robust, we have adapted an Approximated Maximum Likelihood technique coupled with a generalized Kalman filter.

PACS numbers: 43.30.Es, 43.60.-c, 47.80.+v, 43.60.Qv

I. INTRODUCTION

In several areas of fluid dynamics research, it is desirable to study the motion individual fluid particles in a flow, i.e. the Lagrangian dynamics of the flow. The properties of this motion governs the physics of mixing, the behavior of binary flows and the Eulerian complexity of chaotic and turbulent flows. Lagrangian studies are possible in numerical experiments where chaotic¹ and turbulent^{2,3,4,5} flows have been studied. For turbulence, the numerical studies are limited to small Reynolds number flows whose evolution is only followed during a few large-eddy turnover times. In addition only the small scales properties of homogeneous turbulence are captured; the influence of inhomogeneities (such as large scale coherent structures) are not taken into account. It does not seem possible at the moment to extend high resolution turbulent DNS computations to long periods of time or to high Reynolds number flows. Experimental studies are thus needed. They differ from the numerical studies because one cannot tag and follow individual *fluid* particles; most techniques aim at recording the motion of *solid* particles carried by the flow motion. The degree of fidelity with which solid particles can act as Lagrangian tracers is an open problem; it depends on the size and density of the particle. While the interaction between the particle and its wake can be important for large particles or particles with a large density difference with the surrounding fluid^{6,7,8}, it is generally admitted that density matched particles with a size smaller than the Kolmogorov length follow the fluid. Measurements of small particle motion have been made, using optical techniques that follow individual particle motion over short times/distances^{9,10}. We propose here an acoustic technique that can resolve an individual particle motion over long periods of time (compared with the characteristic time of flow forcing).

The principle of the technique is to monitor the Doppler shift of the sound scattered by a particle which is *continuously* insonified. This is an extension of the pulsed Doppler method that has been developed to measure velocity profiles and that has many applications in fluid mechanics and medicine¹¹. The main advantage of the continuous insonification is to improve the time resolution of the measurement, although it is limited to the tracking of a very small number of particles (the tests reported here are made with only one particle in the flow). The measurement relies on the ability to track a Doppler frequency and its variation in time. For this signal processing problem two classes of approaches have been developed: (i) time-frequency analysis and (ii) high resolution parametric spectral analysis. Time frequency methods mainly rely upon the quadratic Wigner-Ville transform, or smoothed versions of it. Numerous studies and papers have recently been published, in which the theoretical issues are presented (see e.g. the textbooks by Flandrin¹² or Cohen¹³). These non parametric techniques are convenient and well-suited for weakly non-stationary signals with a good signal-to-noise ratio (SNR). However, time frequency representations present numerous

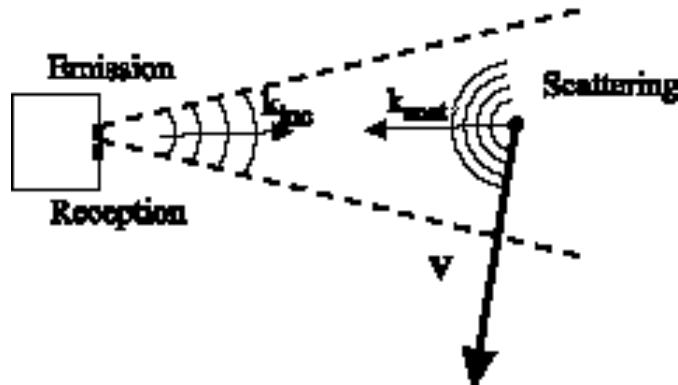


FIG. 1: Principle of measurement. A large 3D measurement zone is achieved by using a transducer size of a few wavelengths.

drawbacks when it comes to extract trajectory information. Their quadratic nature give rise to numerous spurious interference terms that require post processing. For signals with a faster frequency modulation and a low SNR, we show here that an optimized parametric approach is a better choice. Parametric high resolution spectral analysis methods take advantage of an a priori knowledge of the spectral content of the recorded signal, namely the emitted signal frequency plus one or many doppler-shifted echoes. Furthermore, a time-recursive frame for the estimation of the Doppler shift is proposed here, where the evolution of the frequency is taken into account in the algorithm.

The two methods are tested in two experiments, in which the acoustic signals have different time scales and noise levels. The first experiment is a study of the transient acceleration of a heavy sphere settling under gravity in a fluid at rest. In this case the characteristic time scale of velocity variations is slow ($\tau \sim 50$ ms) and the signal to noise ratio is fair (about 20 dB); we show that a technique of reassignment of the spectrogram gives good results. The second experiments deals with the motion of a neutrally buoyant sphere embedded in a turbulent flow. In this case, velocity variations occur over times of about 1 ms and the signal to noise ratio is low (less than 6 dB). We show that the AML parametric method yields very good results in that situation.

The paper is organized as follows: in section II we present the acoustic technique and measurement procedure. In section III we describe the signal processing techniques, with a particular emphasis on the AML method which has been developed and optimized to this particle tracking problem. Examples of applications to measurements in real flows are given in section IV.

II. ACOUSTICAL SET-UP

A. Principle of the measurement

In the experimental technique proposed here, a particle is continuously insonified. It scatters a sound wave whose frequency is shifted from the incoming sound frequency due to the Doppler effect. This Doppler shift is directly related to the particle velocity \mathbf{v}_p :

$$\Delta\omega = \mathbf{q} \cdot \mathbf{v}_p \quad , \quad (1)$$

where \mathbf{q} is the scattering wavevector (the difference between the incident and scattered wavevectors $\mathbf{q} = \mathbf{k}_{\text{scat}} - \mathbf{k}_{\text{inc}}$) and ω is the wave pulsation.

We choose a backscattering geometry (see figure 1) so that $\mathbf{q} = -2\mathbf{k}_{\text{inc}}$ and the frequency shift becomes

$$\Delta\omega(t) = -2\frac{v(t)}{c}\omega_0 \quad , \quad (2)$$

where c is the speed of sound, ω_0 is the incident pulsation, and $v(t)$ is the component of the velocity on the incident direction at time t . We continuously insonify the moving particle and record the scattered sound. If need be, the particle position can be obtained by numerical integration of the velocity signal.

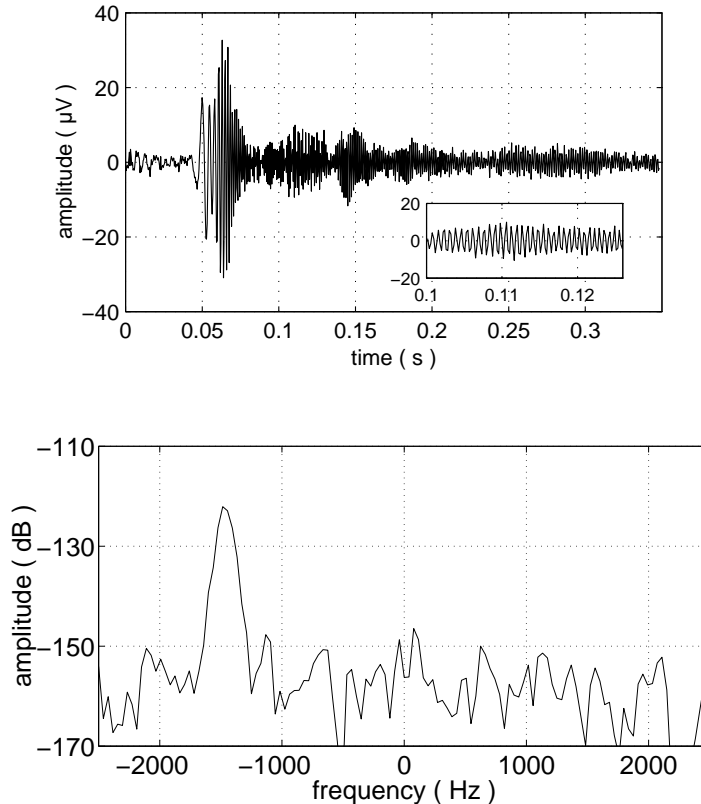


FIG. 2: Data from a steel bead (diameter 1 mm) settling in water at rest. (a) Typical time series; (b) power spectral density of the inset figure. On the x-axis, zero corresponds to the emission frequency.

B. Transducers characteristics and acquisition

We use a Vermon array of ultrasonic transducers made of individual elements of size 2×2 mm each, separated by $100 \mu\text{m}$. Their resonant frequency is about 3.2 MHz and their bandwidth at -3 dB is 1.5 MHz. Sound emission is set at 3 MHz or 3.5 MHz; experiments are performed in water so that the wavelength is $\lambda = 0.50$ mm or 0.43 mm. The corresponding emission cone for each $d = 2$ mm square element is 29° at 3 MHz and 24° at 3.5 MHz. In our measurements, the particle to transducer distance lies between 5 cm and 40 cm, so that measurements are made in the far field ($d^2/\lambda > 10$ mm). Given maximum flow and particle velocities of the order of $1.5 \text{ m}\cdot\text{s}^{-1}$, we expect a maximum sound frequency shift of the order of 5 kHz or 6 kHz, depending on whether the emission is at 3 MHz or 3.5 MHz. This yields a frequency modulation rate of at most 0.25%. One element of the transducer array is used for continuous sound emission and another for scattered sound detection. As the operation is continuous (as opposed to pulsed) and the elements are located close to one-another, we observe a coupling between the emitter and the receiver of the order of 60 dB (this is due both to electromagnetic and acoustic surface waves cross-talk).

The sound scattered by the moving particle is detected by a piezoelectric transducer. Upon connection to a 50Ω impedance, it yields an electrical signal of about 2 to 30 μV . In comparison, the noise is 1 μV and the electromagnetic coupling with the emitter is 8 mV. Hence the signal to noise ratio is between 0 dB and 30 dB. The transducer output is sampled at 10 MHz over a 21 bit dynamical range (input range 31.25 mV) and numerically heterodyned at the emitting frequency. Then it is decimated at the final sampling frequency of 19531 Hz. The acquisition device is a HP-e1430A VXI digitizer.

C. Scattering by an elastic sphere

The study of sound scattered by a fixed solid sphere is a classic but continuing area of study and difficulties arise in the interpretation of observed phenomena especially when trying to deal with elasticity and absorption^{14,15,16}.

Complex behaviour is observed linked with resonances of Rayleigh waves at the surface of the sphere. As a consequence the scattered pressure distribution varies both in directivity and amplitude. A generic expression for the far field pressure is the following :

$$p_{scat}(r, \theta) = p_{inc} \frac{af(ka, \theta)}{2r} e^{ikr} , \quad (3)$$

where r is the distance from the center of the sphere, a its radius, p_{inc} the incident pressure on the sphere, k the incident wavenumber in the fluid, θ the scattering angle and f is a form function which depends on the physical properties of the solid medium. Under very general assumptions, f can be developed as a series of partial waves:

$$f(ka, \theta) = \frac{2}{ika} \sum_{n=0}^{\infty} (2n+1) \frac{B_n(ka)}{D_n(ka)} P_n(\cos \theta) , \quad (4)$$

where P_n is the a Legendre polynomial, B_n and D_n are determinants of matrices composed of spherical Bessel and Hankel function and their derivatives¹⁴. Physically, f represents the sum of the specular echo and of interferences due to the radiation by Rayleigh waves^{15,16}. As a result, f is a strongly varying function, particularly for high values of ka . In our experiments we used spheres of different material (polypropylene PP, steel, tungsten carbide, glass) with corresponding ka between 7 and 15. The flow acts on the sphere motion, thus causing its acceleration and, eventually, its rotation. These effects may change the radiation diagram: first there is Doppler shift for the sound received by the sphere, and, perhaps more importantly, the sphere rotation may change the Rayleigh emission. For these reasons, the evolution of the amplitude of the scattered sound during the particle motion is quite complex. However, the observed amplitude modulation (see figures 2 and 8) varies slowly enough to allow a correct estimate of the frequency modulation of the scattered sound.

III. SIGNAL PROCESSING

Numerous spectral estimation techniques are based on the ideas behind Fourier analysis of linear time invariant (LTI) differential equations. These techniques may be divided into (i) non-parametric techniques where the basis functions are implicitly the harmonically related complex exponentials of Fourier analysis and (ii) parametric techniques whose task is the estimation of the parameters of a (sub)set of complex exponentials. The spectrogram and the reassigned spectrogram belong the former category, whereas the maximum likelihood and its approximate form belong to the latter.

A. Time-Frequency analysis

The most common time frequency distribution (TFD), the spectrogram, involves a moving time window. This window attempts to capture a portion of the signal which is sufficiently restricted in time so that stationarity and LTI assumptions are approximately met. To overcome the inherently poor localization in the time-frequency plane, a method has been proposed by Gendrin et al.¹⁷, and extended more recently by Auger and Flandrin^{12,18}. The idea is to locally reassign the energy distribution to the local center of gravity of the Fourier transform. Despite its ability to exhibit clear and well localized trajectories in the time-frequency plane, this technique requires an additional image processing step to extract the TF trajectory. For rapidly fluctuating frequency modulations and/or low SNR spurious clusters appear which makes this extraction difficult. The parametric method presented below is more robust.

B. AML spectral estimation

This approach is largely based upon maximum likelihood spectral estimation (see e.g. Kay¹⁹). The fundamentals are briefly recalled, as they serve as a basis for the approximate likelihood scheme, originally developed by Clergeot and Tressens²⁰. This work is extended here within a recursive estimation frame, thus allowing to track the variations of the Doppler frequency shift induced by fast velocity changes of a scattering sphere imbedded in a turbulent flow. Michel and Clergeot have developed a similar approach for non stationary spectral analysis in an array processing frame^{21,22}.

1. Introduction

In this section, we address the problem of estimating the frequencies f_1, \dots, f_M of M harmonic signals embedded in noise, from a small number of samples

$$x(t) = \sum_{m=1}^M a_m(t) \exp(j(2\pi f_m t + \phi_m)) + n(t). \quad (5)$$

As the number of sampling points that are supposed to be available is low, classical Fourier based approaches fail to provide good results. We focus our attention on parametric approach, where an a priori knowledge about the structure of the signal is taken into account to improve the analysis.

The following assumptions are made:

- The time series is regularly sampled with time period T_s , so as to insure $\frac{1}{T_s} > \frac{f_{max}}{2}$ where f_{max} stands for the bandwidth of the anti-aliasing filter used in the recording process. For convenience, T_s will be set to $T_s = 1$ and the term *frequency* will refer to *normalized* frequency (i.e. the actual frequency, divided by $F_s = \frac{1}{T_s}$).
- The amplitudes $a_i(t)$ are deterministic but unknown.
- The noise is a complex white gaussian circular and iid (independent increment identically distributed) with (unknown) variance σ^2 ; the distribution function of a k -dimensional vector \vec{N} defined by

$$\vec{N}(t) = [n(t), n(t+1), n(t+2), \dots, n(t+(K-1))]^T \quad (6)$$

reads

$$p(\vec{N}) = \frac{1}{(\sqrt{2\pi}\sigma)^K} \exp\left(-\frac{|\vec{N}|^2}{2\sigma^2}\right). \quad (7)$$

Furthermore, the noise and the signal are independent.

- The term *observation* refers to a set of Q K -dimensional vectors constructed from the sampled time series, according to

$$\vec{X}(t_j) = [x(t_j), x(t_j+1), x(t_j+2), \dots, x(t_j+(K-1))]^T \quad j = 1, \dots, Q \quad (8)$$

- The frequency f is supposed to remain constant during an observation.

Under the assumption that the noise process is iid, and that the observed vectors are corrupted by independent realizations of the noise process, the likelihood of the observation is given by the product of the likelihood of each vector. Let \mathcal{P} be the set of searched parameters (\mathcal{P} contains σ^2 , $F = \{f_1, \dots, f_M\}$ and the $\vec{A} = [a_1 \exp(j\phi_1), \dots, a_M \exp(j\phi_M)]^T$), the loglikelihood of an observation is simply given by

$$\mathcal{L}(\mathcal{P}) = -KQ \log(2\pi\sigma^2) - \frac{1}{2\sigma^2} \sum_{q=1}^Q |\vec{X}(q) - \mathbf{S}(\vec{F})\vec{A}(q)|^2, \quad (9)$$

where

$$\mathbf{S}(\vec{F}) = [\vec{S}_1, \dots, \vec{S}_M] = \begin{pmatrix} 1 & \exp(2\pi f_1) & \dots & \exp(2\pi(K-1)f_1) \\ \vdots & & & \vdots \\ 1 & \exp(2\pi f_M) & \dots & \exp(2\pi(K-1)f_M) \end{pmatrix}^T. \quad (10)$$

According to the maximum likelihood principle, the set \mathcal{P} of parameters must be chosen in order to maximize expression (9).

2. Reduced expression

Minimizing (9) jointly for all the parameters is usually untractable. Most authors propose a separate maximisation for each of the parameters. For our application, the spectral components (i.e. \vec{A} and \vec{F}) are the relevant variables. We first maximize with respect to \vec{A} and derive an expression for the optimal \vec{F} ; σ^2 is estimated independently.

The value of vector \vec{A} which minimizes the norm $|\vec{X}(q) - \mathbf{S}(\vec{F})\vec{A}(q)|^2$ is easily obtained :

$$\vec{A}(q) = (\mathbf{S}^+\mathbf{S})^{-1}\mathbf{S}^+(\vec{F})\vec{X}(q) . \quad (11)$$

Note that the ‘‘signal only’’ vector $\vec{Y} = \vec{X} - \vec{N}$ appears to be the orthogonal projection of \vec{X} on the signal subspace spanned by the row vectors of \mathbf{S} :

$$\vec{Y} = \mathbf{S}(\vec{F})\vec{A}(q) = \mathbf{S}((\mathbf{S}^+\mathbf{S})^{-1}\mathbf{S}^+(\vec{F})\vec{X}) = \Pi_s(\vec{F})\vec{X} , \quad (12)$$

where $\Pi_s(\vec{F})$ stands for the parametric projector on the signal subspace²⁷. Let $\Pi_n(\vec{F}) = \mathbf{I} - \Pi_s(\vec{F})$ be the noise subspace, \mathbf{I} is the identity matrix. By substituting (12) and using the definition of $\Pi_n(\vec{F})$ in the expression of the log-likelihood (9), one gets the following simplified expression to minimise

$$L(\vec{F}) = \frac{1}{\sigma^2} \sum_{q=1}^Q |\Pi_n(\vec{F})\vec{X}|^2 . \quad (13)$$

Using the properties of the trace operator (hereafter denoted Tr) and those of the projection matrix $\Pi_n(\vec{F})$, the maximum likelihood estimation of \vec{F} takes the common form : minimize

$$L(\vec{F}) = \frac{Q}{\sigma^2} \text{Tr} \left[\Pi_n(\vec{F})\hat{\mathbf{R}}_x \right] , \quad (14)$$

where $\hat{\mathbf{R}}_x$ is an estimate of the correlation matrix \mathbf{R}_x of the vector process $\vec{X}(q)$. Minimizing $L(\vec{F})$ in (14) leads to the exact value \vec{F}_{ML} which has the maximum likelihood. It is important here to emphasize the following : if the vectors \vec{X} are obtained by time-shift over the recorded time series, an observation runs over $K + Q - 1$ samples, i.e. the actual duration of one observation is $T_{obs} = (Q + K - 2)T_s$. In this case, the observed vectors may not be considered as being corrupted by independent realisations of the noise process, as some ‘time integration’ is performed in the estimation of \mathbf{R}_x . The consequences and interest of such smoothing have been studied by Clergeot and Tressens²⁰, and Ouamri²³, in the frame of array processing (in this context, ‘time integration’ becomes ‘spatial smoothing’). In the remainder of this paper, the development are based on equation (14), no matter how \mathbf{R}_x is estimated; see appendix for the practical implementation.

3. Approximate Max-likelihood

Equation (14) is still too complicated to be solved analytically in a simple way. A minimization can be easily performed if $L(\vec{F})$ has a quadratic dependance in \mathbf{S}^{20} . Let \mathbf{R}_y be the correlation matrix of the signal vectors $\vec{Y}(q)$, the assumption that signal and noise are independent allow to establish the following equalities

$$\hat{\mathbf{R}}_x = \mathbf{R}_y + \hat{\sigma}^2\mathbf{I} , \quad (15)$$

$$\mathbf{R}_y = \mathbf{S}\mathbf{P}\mathbf{S}^+ , \quad (16)$$

$$\mathbf{P} = \mathcal{E}[\vec{A}\vec{A}^+] , \quad (17)$$

where \mathcal{E} stands for the mathematical expectation. Substituting in equation (14) leads to:

$$L(\vec{F}) = \frac{Q}{\hat{\sigma}^2} \text{Tr} \left[\Pi_n(\vec{F})\hat{\mathbf{S}}\mathbf{P}\hat{\mathbf{S}}^+ \right] . \quad (18)$$

Clergeot and Tressens²⁰ propose a second order approximation of $L(\vec{F})$:

$$L_{AML}(\vec{F}) = \frac{Q}{\hat{\sigma}^2} \text{Tr} \left[\hat{\Pi}_n\hat{\mathbf{S}}(\vec{F})\hat{\mathbf{P}}\hat{\mathbf{S}}^+(\vec{F}) \right] , \quad (19)$$

in which $\hat{\Pi}_n$ is estimated by computing the projector spanned by the $(K - N)$ smallest eigenvalues of the estimated covariance matrix $\hat{\mathbf{R}}_x$. They prove that this approach leads to more reliable estimates of \vec{F} at low signal to noise ratio (SNR), and that the minimization of L_{AML} is asymptotically efficient. In practice, the following set of equations is used

$$\hat{\sigma}^2 = \frac{1}{K - M} \text{Tr}(\hat{\Pi}_n \hat{\mathbf{R}}_x), \quad (20)$$

$$\Pi_s(\vec{F}) = \mathbf{S}(\vec{F})(\mathbf{S}^+(\vec{F}) \cdot \mathbf{S}(\vec{F}))^{-1} \cdot \mathbf{S}^+(\vec{F}), \quad (21)$$

$$\mathbf{S}(\vec{F}) \cdot \hat{\mathbf{P}} \cdot \mathbf{S}^+(\vec{F}) = \Pi_s(\vec{F})(\hat{\mathbf{R}}_x - \sigma^2 \mathbf{I}) \cdot \Pi_s(\vec{F}). \quad (22)$$

The approximately quadratic dependence of L_{AML} in $\mathbf{S}(\vec{F})$, allows a fast convergence of the minimization algorithm by using a simple Newton-Gauss algorithm:

$$\vec{F}(k+1) = \vec{F}(k) - \mathbf{H}^{-1} \cdot \vec{\text{grad}}(L_{AML})|_{\vec{F}=\vec{F}(k)}, \quad (23)$$

where k stands for the iteration step in the minimization process, $\vec{\text{grad}}$ and \mathbf{H} are the gradient and hessian respectively (see expressions in the appendix).

4. Combining new measurements and estimates

In this section, it is assumed that new measurements do not allow by itself the derivation of a good estimate. The variance of such an estimate varies as $\frac{1}{T_{obs}} \simeq (K + Q - 1)^{-1}$, whereas integrating new measurements to this estimate allow to derive a better estimation.

Let $\hat{\vec{F}}(t)$ be an estimate of \vec{F} at time t , and $\mathcal{N}(\hat{\vec{F}}(t), \Gamma(t))$ its density, assumed to be normal with variance $\Gamma(t)$ ²⁸. If a linear evolution model is known for $\vec{F}(t)$, one has

$$\vec{F}(t+1) = \mathbf{M}\vec{F}(t) + \varepsilon(t), \quad (24)$$

$$p_{t+1|t}(\vec{F}) = \mathcal{N}(\mathbf{M}\hat{\vec{F}}(t), \mathbf{M}\Gamma(t)\mathbf{M}^+ + \mathbf{R}_\varepsilon), \quad (25)$$

where \mathbf{M} is the evolution matrix; ε is a perturbation term, which is statistically independent from \vec{F} , and \mathbf{R}_ε is its covariance matrix. $p_{t+1|t}$ is the probability density function that can be derived for time $t+1$, if the observations are made until time t only. As such an evolution equation is usually unknown, \mathbf{M} will be set to the identity matrix in the rest of the paper (see Michel²²) for a detailed discussion). Applying the Bayes rule over conditional probabilities gives :

$$p_{t+1|t+1}(\vec{F}) = \frac{p_{t+1|t}(\vec{F}) \cdot p_{t+1}(\vec{X}|\vec{F})}{p_{t+1}(\vec{X})}. \quad (26)$$

Noting that $\log(p_{t+1}(\vec{X}|\vec{F}))$ is the loglikelihood function for which a reduced expression has been derived in the previous section, one gets after all reductions and identifications the simple following expressions

$$\hat{\vec{F}}(t+1|t) = \hat{\vec{F}}(t), \quad (27)$$

$$\Gamma(t+1|t) = \Gamma(t) + \mathbf{R}_\varepsilon, \quad (28)$$

$$\Gamma(t+1)^{-1} = \mathbf{H} + \Gamma(t+1|t)^{-1}, \quad (29)$$

$$\hat{\vec{F}}(t+1|t+1) = \hat{\vec{F}}(t+1) = \hat{\vec{F}}(t+1|t) - \Gamma(t+1)^{-1} \cdot \vec{\text{grad}}, \quad (30)$$

where it can be shown that the gradient function has the same expression as in the previous section. \mathbf{R}_ε is an unknown matrix which will be practically set to $v^2 \mathbf{I}$, where v^2 will be tuned in order to allow the algorithm to take slight changes in \vec{F} into account. Furthermore, it is interesting that the set of expression above expresses a generalized Kalman filter for estimating \vec{F} (in the sense that it relies upon second order expansion of the loglikelihood functions). The statistical convergence properties and numerical efficiency of these approaches are described in the work of Michel & Clergeot²¹ and Michel²².

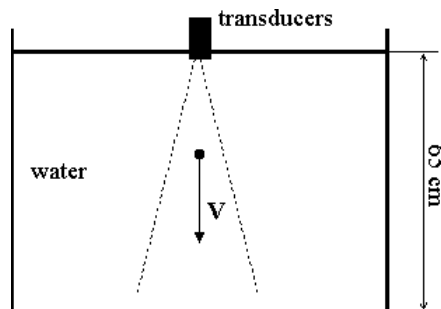


FIG. 3: Experimental setup in the case of the settling sphere.

IV. EXPERIMENTAL RESULTS

We first describe the simple case of a particle settling in a fluid at rest. It is well adapted to the reassigned spectrogram method because the acoustic signal has a good SNR and a slow frequency modulation. We show that it allows to extract the subtle interaction between the falling particle and its wake. We then study the more complicated case of the motion of a particle embedded in a turbulent flow, where the dynamics of motion is much faster and the SNR is poor. We show that the AML method is well suited.

A. The settling sphere

1. Motivation and experimental setup

When a particle is released in a fluid at rest, its developing motion creates a wake. The particle velocity is then set by the balance between buoyancy forces and drag, and additional subtle effects: first, ‘added mass’ corrections because the particles ‘pushes’ the fluid, and second, a ‘history’ force because the wake reacts back on the particle. Formally, one can write the equation of motion as^{6,8,24}:

$$(m_p + \frac{1}{2}m_f)\frac{d\mathbf{v}_p}{dt} = (m_p - m_f)\mathbf{g} - \frac{1}{2}\pi a^2 \rho_f \|\mathbf{v}_p\| \mathbf{v}_p c_D(Re) + \mathbf{F}_{\text{history}} \quad (31)$$

where m_p is the particle mass, m_f is the mass of a fluid particle of the same size, v_p is the particle velocity, \mathbf{g} is the acceleration of gravity, a is the sphere radius, ρ_f is the fluid density, c_D is the static empiric drag coefficient, Re is the Reynolds number $Re = \frac{2av_p}{\nu}$ and $\mathbf{F}_{\text{history}}$ is the so-called history force. In this expression, the drag coefficient is usually obtained from measurement of the forces acting on a body at rest in an hydrodynamic tunnel. The history term, however, is largely unknown. Analytic expression can only be derived in the limit of small Reynolds numbers (less than 10) and cannot be applied for real flow configurations (e.g. multiphase flows) where $Re \gg 1$.

We perform measurements of the motion of a settling sphere, with the aim of evaluating the influence of the history forces. We use a water tank of size 1.1 m×0.75 m and depth 0.65 m, filled with water at rest (figure 3). The bead is held by a pair of tweezers, five centimeters below the transducers. It is released a time $t=0$ without initial velocity and its trajectory is about 50 cm long. The data acquisition is started before the bead is released in order to capture the onset of motion.

2. Results

Let us use as a first example, the fall of steel bead, 0.8 mm in diameter. The Doppler shift during the bead motion is detected using the spectrogram representation and a subsequent reassignment scheme. The simple spectrogram and reassigned version are shown in figure 4. The reassignment technique drastically improves the localization of the energy in the time-frequency plane. In this case, the image processing step computes $v_p(t)$ as the line of maxima. The precision of the overall measurement depends on two factors : first on the intrinsic precision of the reassignment method and second on the dispersion of the measurements (the reproducibility of the bead motion over several experiments). The intrinsic precision of the reassignment method has been empirically studied using synthetic signals modelling the particle dynamics plus a noise that mimics the experimental data. We observed that for our choice of

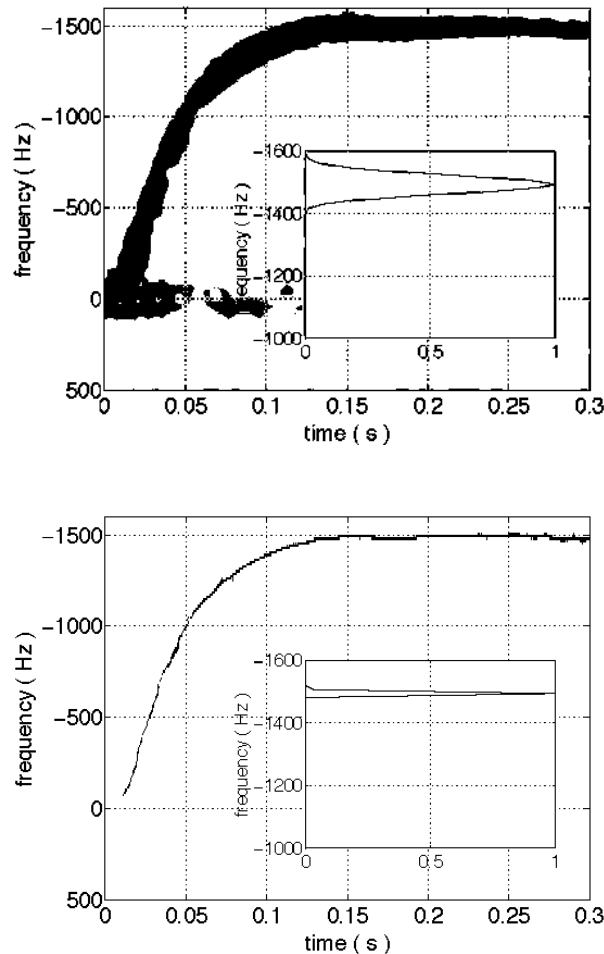


FIG. 4: (a) Spectrogram of the backscattered sound, after heterodyne detection. (b) Reassigned spectrogram. In each figure the inset shows a normalized cross-section of the spectrogram. The algorithm is that of the `tfrresp` function of the MATLAB time-frequency toolbox²⁵. To get rid of the spectral components at zero frequency due to the coupling between transducers and at small frequencies around zero due to slow motion of the water surface, we use a high pass fifth order Butterworth filter of cut-off frequency 25 Hz (corresponding to a velocity of 5 mm/s). Data of 0.8 mm steel bead settling in water at rest.

parameters (a time-frequency picture with 256×256 pixels) the *rms* precision is about one half pixel both in time and frequency directions. The method thus allows a precise analysis of the dynamics of the fall; we describe below two sets of experiment that illustrate the potential of the reassignment technique.

First, we show in figure 5 the velocity of a 1 mm steel bead (average over ten falls) together with two numerical simulations based on equation 31, first without the memory force and second with the expression of the memory force derived at low Reynolds numbers (called the Stokes memory term, as in Maxey & Riley⁶). The precision of the detection technique is sufficient for the measured profile to be compared to the simulated curves and to draw physical conclusions about the hydrodynamical forces. At early times, the trajectory is close to the simulation with memory force. This is due to the diffusion away from the bead surface of the vorticity generated at the boundary^{6,8,24}. However, as the instantaneous Reynolds number increases, the curve deviates from this simple regime: vorticity is advected into the wake. Memory is progressively lost and the sphere reaches a terminal velocity in a finite time as does the simulation without memory.

The measurement and signal processing techniques are then tested on a more non-stationary motion, as in the case of a bead whose density is close to that of the fluid. In this situation a stronger interaction is expected between the particle motion and the development of its wake. Formally, this traces back to differences in the effective inertial mass and buoyancy mass of the particle – see equation (31). In figure 6, we show the velocity variation for a light glass sphere (density 2.48) compared to a tungsten bead (density 14.8). We observe that the velocity of the glass oscillates before reaching a constant terminal value whereas the other particle has a regular acceleration. In the case of light

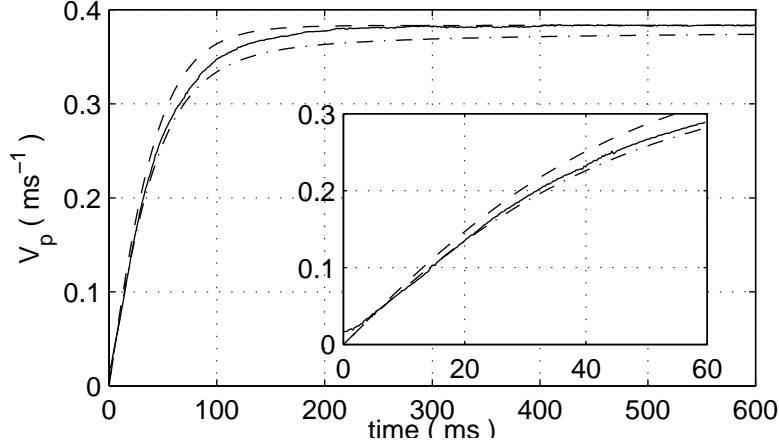


FIG. 5: Velocity measurement of a steel bead of diameter 1 mm (solid line), compared to numerical simulations without memory force (dashed) and with Stokes memory (dash-dotted). The inset shows an enlargement near the onset of motion. The Reynolds number, based on the limit velocity is 430. The sphere velocity profile results from averaging $n = 10$ successive experiments.

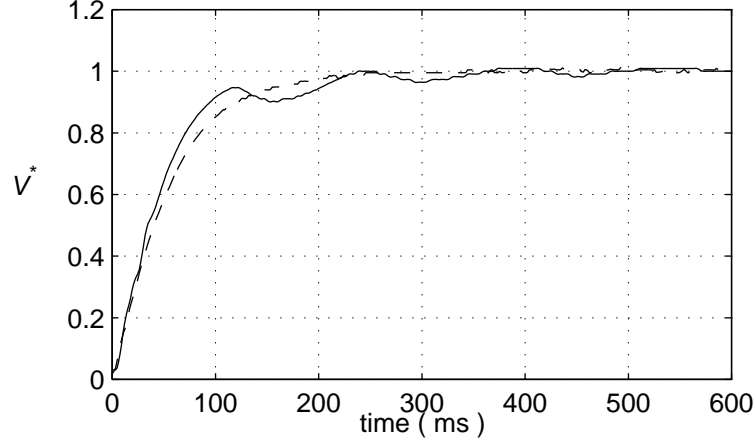


FIG. 6: Fall of a tungsten carbide sphere $D=1$ mm (dashed) compared to a glass bead $D=2$ mm (solid), at $Re \sim 400$. The velocity is non-dimensionalized by the limit velocity. Curves are not averaged over several experiments.

beads the hydrodynamic forces may be large enough to overcome the gravity and change the sign of the acceleration. This is linked with the non-stationarity of the wake, as vortex shedding is known to occur for Reynolds number above critical ($Re_c \sim 250$).

B. Turbulent flow : Lagrangian velocity measurement

1. Experimental set-up

The turbulent flow is generated in a von Kármán geometry : the water is set into motion by two coaxial counter rotating disk in a cylindrical tank (figure 7). The Reynolds number $Re = \frac{2\pi R^2 f}{\nu}$ (where $\nu = 0.8910^{-6} \text{ m}^2\text{s}^{-1}$ is the water kinematic viscosity) is equal to 10^6 . To prevent cavitation in the flow, we boil the water before filling the tank by lowering the pressure with a vacuum pump and during the experiment the pressure is increased to two bars. For the acoustic measurement, we use the same array of transducers as in the previous experiments, at emitting frequency 3 MHz. The cylinder and the surface of the disks are covered by 3 cm of Ciba Ureol 5073A and 6414B. Its density is 1.1 and the sound velocity is $1460 \text{ m}\cdot\text{s}^{-1}$ so that its acoustic impedance is close to that of the water, reducing drastically the reflections at the interface water/ureol compared to water/steel. The attenuation at 2.5 MHz is about 6 dB per cm. With a 3 cm layer and after the reflection on steel the total absorption is about 36 dB. The total

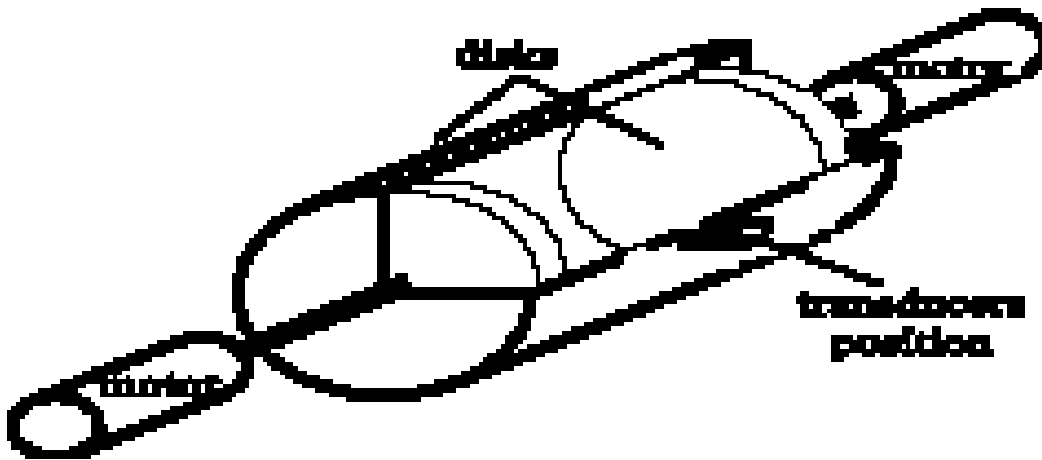


FIG. 7: Experimental setup. The inner radius of the cylinder is 10 cm (disks radius $R=9.5$ cm) and the distance between the disks is 18 cm. The disks are driven by two 1 kW motors at a constant rotation frequency of $f=18$ Hz. The transducers are placed 18 cm off axis, in order to increase the volume of the measurement region.

reflection at the interfaces is reduced by a factor 60. The particle is a polypropylene (PP) sphere of radius 1 mm and density 0.9.

2. Results

We show in figure 8 the time series when one particle is in the ultrasonic beam and the corresponding spectrogram and reassigned spectrogram. The signal to noise ratio is very poor, typically less than 6dB (to give an idea, in figure 8(a) the bead enters the ultrasonic beam at $t \sim 20$ ms). One can also see some events localized in the time frequency plane that may be considered as noise and that may have several origin (noise of the motors, external electromagnetic noise, cavitation in the flow. . .). Altogether, the time-frequency pictures show the trajectory of the particle but the low SNR prevents it from being easily extracted. In particular, the trajectory in the reassigned picture becomes quite lacunar and extracting it would require sophisticated (and CPU greedy) image processing techniques.

The result of the AML algorithm is plotted in figure 9. The extracted frequency modulation is of course within the estimation in the spectrogram as in figure 8(b), but one observes that fine variations in the velocity of the bead are now detected. The algorithm provides also an estimate of the amplitude of the source (figure 9(c)). It can be seen that there is a strong amplitude modulation and that the SNR is at most 6 dB and may become less than 0 dB.

As the hessian is related to the Fisher information matrix²⁶, its inverse square root is linked with the variance of the estimation: a large value of the hessian indicates an accurate estimation of the modulation frequency and, hence, of the bead velocity. The inverse square root of the hessian is plotted in figure 9(b): very large values are calculated in the absence of a bead in the measurement volume at the beginning and end of the time series (as a signature of the mismatch between the model which is composed of one source at least and the reality: no source). Local lower values (typically less than 0.1) are observed when the variance on the estimation is small. Spurious effects are generated when the frequency modulation approaches zero as the hessian also becomes very small because of the filtering operation made in order to get rid of the coupling part of the signal. Finally, one observes that the hessian decreases as the signal to noise ratio increases (see at time 0.55 s).

V. CONCLUDING REMARKS

As can be seen in the previous section, both methods, time-frequency analysis and parametric spectral analysis are suited for extracting the time-varying frequency modulation due to a Doppler effect. The domain of application of each method depends on the degree of non-stationarity and on the SNR.

For high SNR and weakly non-stationary signals, the time-frequency approach yields very good results. One drawback is the need of a second processing stage to extract the trajectory from the time-frequency picture. This stage may become increasingly difficult if there is more than one spectral component or if the SNR degrades. In both cases the quadratic nature of the algorithm produces interference patterns in the image: spurious clusters and

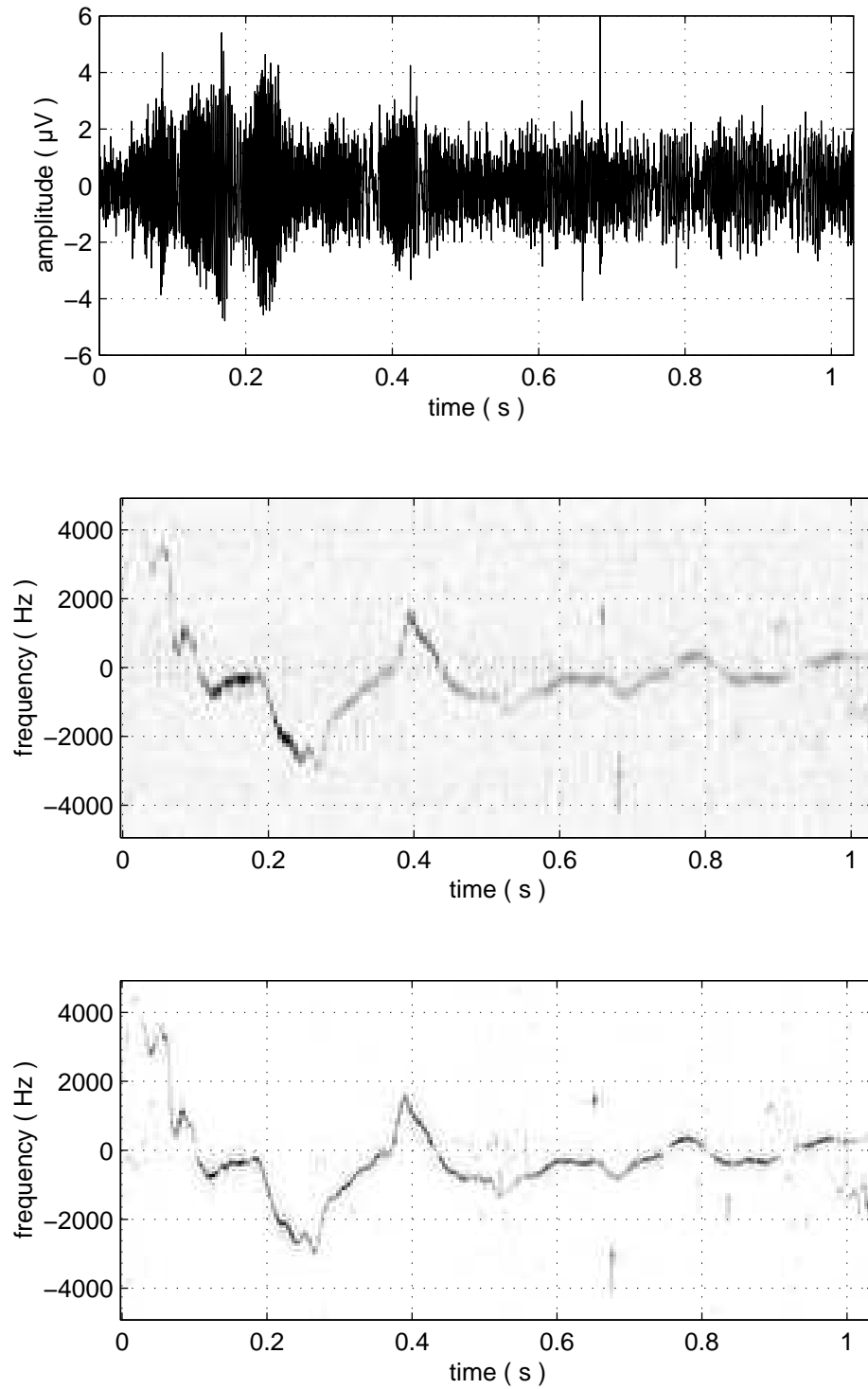


FIG. 8: Sound scattered by a 2 mm diameter PP bead in a turbulent flow at $Re = 10^6$. (a) Typical time series; (b) and (c) corresponding spectrogram and reassigned spectrogram.

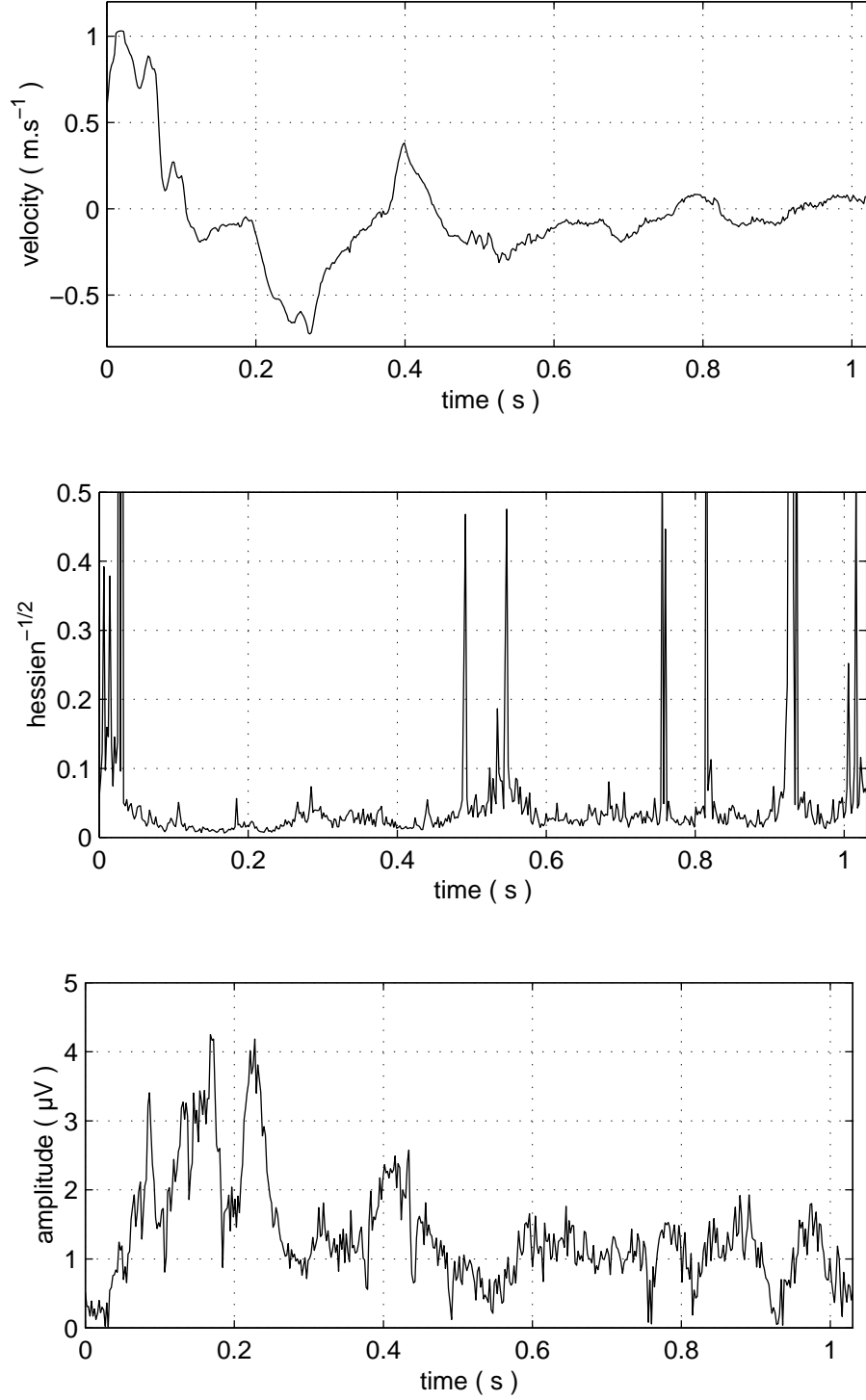


FIG. 9: Velocity measurement for the motion of a 2 mm diameter PP bead in a turbulent flow at $Re = 10^6$. Output of the AML algorithm: (a) velocity (b) corresponding inverse square root of the hessian, (c) amplitude of the source (the rms value of the noise is $0.9\mu\text{V}$). AML algorithm parameters: $M=1$, $K=7$, $Q=13$, $v^2=10^{-5}$.

a lacunar trajectory result. Another, more fundamental, limitation is that the length of the time window must be long enough to preserve an acceptable frequency resolution, even with the reassigned spectrogram. This limits the methods to weakly non-stationary signals.

For signals with a rapid frequency modulation, the AML spectral estimation is well suited, as long as the noise is near iid. The size of the time window can be decreased because of the parametric nature of the method, since *a priori* knowledge has been taken into account. The performance is further increased by the use of a Kalman-like filter. The drawback is the necessity to find a good dynamical model for the evolution of the spectral components. We have chosen here the simplest model which works well for our experiments but the approach can be refined by increasing the number of parameters in order to consider more precisely the variation of the frequency. The AML algorithm also provides a quantitative estimation of the quality of the demodulation and the instantaneous power of the spectral component. Finally, the AML method has the advantage to provide directly frequency modulation as a function of time, in one stage.

Acknowledgments

We are indebted to Pascal Metz for the development of the signal conditioning electronics. We thank Marc Moulin for his help in the design of the von Kármán setup, VERMON for continuous assistance in the development of the transducer array. This work is partially supported by ACI grant No. 2226.

AML ALGORITHM

- First step : calculate $\hat{\mathbf{R}}_x$ using the following expression²² :

$$\hat{\mathbf{R}}_x = \frac{1}{2Q} \sum_{i=t+1}^{t+Q} \left(\vec{X}(i)\vec{X}(i)^T + \tilde{\vec{X}}(i)\tilde{\vec{X}}(i)^T \right), \quad (32)$$

with

$$\tilde{\vec{X}}(i) = [x(i+K-1), x(i+K-2), \dots, x(i)]^{*T}, \quad (33)$$

where * stands for complex conjugate. $\tilde{\vec{X}}$ is the complex conjugate of the time reversed version of \vec{X} .

- Second step : diagonalize $\hat{\mathbf{R}}_x$; one obtains the eigenvectors $(\vec{V}_i)_{i=1..K}$ and eigenvalues $(\lambda_i)_{i=1..K}$ sorted in decreasing order.
- Third step : Compute $\hat{\Pi}_n$ and $\hat{\sigma}^2$, using the set of equations

$$\hat{\Pi}_n = \sum_{i=M+1}^K \vec{V}_i \vec{V}_i^T, \quad (34)$$

$$\hat{\sigma}^2 = \frac{1}{K-M} \text{Tr}(\hat{\Pi}_n \hat{\mathbf{R}}_x) = \frac{1}{K-M} \sum_{i=M+1}^K \lambda_i. \quad (35)$$

- Forth step : choose $\vec{F} = \hat{\vec{F}}(t)$ as candidate value. Compute $\vec{\text{grad}}$ and \mathbf{H} using²¹

$$\vec{\text{grad}} = \frac{2Q}{\sigma^2} \text{Re} \left\{ \text{Diag}(\mathbf{S}'^+(\vec{F}) \cdot \Pi_n(\vec{F}) \cdot \hat{\Pi}_n \cdot \mathbf{S}(\vec{F}) \cdot \hat{\mathbf{P}}) \right\}, \quad (36)$$

$$\mathbf{H} = \frac{2Q}{\sigma^2} \text{Re} \left\{ \text{Diag} \left((\mathbf{S}'^+(\vec{F}) \cdot \Pi_n(\vec{F}) \cdot \hat{\Pi}_n \cdot \Pi_n(\vec{F}) \cdot \mathbf{S}') \right) \star \hat{\mathbf{P}}^* \right\}, \quad (37)$$

where the operator \star stand for the term to term matrix multiplication, and \mathbf{P}^* is the conjugate of \mathbf{P} , and

$$\mathbf{S}' = \left[\frac{d\vec{S}_1}{df_1}, \dots, \frac{d\vec{S}_M}{df_M} \right]^T. \quad (38)$$

- Fifth step : using equations (27) to (30), compute $\hat{\vec{F}}(t+1)$ and $\Gamma(t+1)$.

The initialization of the algorithm is done by either (i) setting an initial value of $\vec{F}(1)$ or (ii) estimating this value using the maxima of the amplitude of the FFT of a small window of signal (of length 64 or 128 samples) and using the iterative algorithm described in section III B 3 to converge towards $\vec{F}(1)$.

For example, the extracted velocity of figure 9 is obtained by starting at the maximum of energy of the signal and applying the algorithm forward and backward in time. The algorithm is stopped as the mean of the inverse square root of the hessian over a window of size 400 samples exceeds 0.5 for more than 400 samples.

- * e-mail : pinton@ens-lyon.fr
- G. O. Fountain, D. V. Khakhar, I. Mezic, and J. M. Ottino, "Chaotic mixing in a bounded 3D flow", *J. Fluid Mech.* **417** (2000).
 - P. K. Yeung and S. B. Pope, "Lagrangian statistics from direct numerical simulations of isotropic turbulence", *J. Fluid Mech.* **207**, 531 (1989).
 - K. D. Squires and J. K. Eaton, "Lagrangian and eulerian statistics obtained from direct numerical simulation of homogeneous turbulence", *Phys. Fluids* **A3**, 130 (1991).
 - P. K. Yeung, "Direct numerical simulation of two-particle relative diffusion in isotropic turbulence", *Phys. Fluids* **6**(10), 3416 (1994).
 - P. K. Yeung, "One- and two-particle lagrangian acceleration correlations in numerically simulated homogeneous turbulence", *Phys. Fluids* **9**(10), 2981 (1997).
 - M. R. Maxey and J. J. Riley, "Equation of motion for a small rigid sphere in a nonuniform flow", *Phys. Fluids* **26**, 883 (1983).
 - G. Sridhar and J. Katz, "Drag and lift forces on microscopic bubbles entrained by a vortex", *Phys. fluids* **7**, 389 (1995).
 - N. Mordant and J.-F. Pinton, "Velocity measurement of a settling sphere", *Eur. Phys. J. B*, in press (2000).
 - M. Virant and T. Dracos, "3D PTV and its application on lagrangian motion", *Meas. Sci. Technol.* **8**, 1539 (1997).
 - G. A. Voth, K. Satyanarayan, and E. Bodenschatz, "Lagrangian acceleration measurements at large Reynolds numbers", *Phys. Fluids* **10**(9), 2268 (1998).
 - O. F. Bay and I. Güler, "Tissue blood flow assessment of pulsed Doppler ultrasound using autoregressive modeling", *J. Med. Syst.* **23**(1), 77 (1999).
 - P. Flandrin, *Time-Frequency / Time Scale analysis*, vol. 10 of *Wavelet analysis and its application* (Academic Press, 1998).
 - L. Cohen, *Time-Frequency analysis* (A. V. Oppenheim Ed., Prentice Hall, 1995).
 - G. Gaunard and H. Uberall, "RST analysis of monostatic and bistatic acoustic echoes from an elastic sphere", *J. Acous. Soc. Am.* **73**(1), 1 (1983).
 - P. D. Thorne, T. J. Brudner, and K. R. Waters, "Time-domain and frequency-domain analysis of acoustic scattering by spheres", *J. Acoust. Soc. Am.* **95**(5), 2478 (1994).
 - B. T. Hefner and P. L. Marston, "Backscattering enhancements associated with subsonic Rayleigh waves on polymer spheres in water : observation and modeling for acrylic spheres", *J. Acoust. Soc. Am.* **107**(4), 1930 (2000).
 - R. Gendrin and C. de Villedary, "Anambiguous determination of fine structures in multicomponents time-varying signals", *Ann. Telecom.* **35**(3-4), 122 (1979).
 - F. Auger and P. Flandrin, "Improving the readability of time-frequency and time-scale representations by the reassignment method", *IEEE Trans. on Signal Processing* **43**, 1068 (1995).
 - S. Kay, *Modern Spectral Estimation, Theory and Application*, Prentice Hall Signal Processing Series (A. V. Oppenheim Ed., Prentice Hall, 1988).
 - H. Clergeot and S. Tressens, "Comparison of two efficient algorithms for HR source tracking: time recursive implementation.", in *ICASSP'90, Albuquerque, USA* (1990).
 - O. Michel and H. Clergeot, "Multiple source tracking using a high resolution method", in *ICASSP'91, Toronto, Canada* (1991), pp. 1277-1280.
 - O. Michel, *Application des méthodes haute résolution à la localisation et la poursuite de sources sonores*, Ph.D. thesis, Université Paris XI, Orsay (1991).
 - A. Ouamri, *Etude des performances des méthodes d'identification à haute résolution et application à l'identification des échos par une antenne linéaire multicapteurs*, Ph.D. thesis, Université Paris-Sud, Orsay (1986).
 - C. J. Lawrence and R. Mei, "Long-time behaviour of the drag on a body in impulsive motion", *J. Fluid Mech.* **283**, 307 (1995).
 - Trademark, The Mathworks Company. The time-frequency toolbox can be downloaded at <http://crttsn.univ-nantes.fr/~auger/tftbftp.html>.
 - L. Scharf, *Statistical signal processing; detection, estimation and time series analysis* (Addison-Wesley, 1991).
 - It is straightforward to establish that $\Pi_s \vec{Y} = \vec{Y}$ for any vector \vec{Y} lying in the signal subspace. Here 'parametric projector' must be understood as the projector calculated for the vector of frequencies \vec{F}

²⁸ This is generally not the case, but this assumption remains valid as long as the loglikelihood is well approximated by its second order expansion around \hat{F} .